

Effects of tidal energy converters on a tidal channel turbulence conditions

V. Ramos*, Patxi Garcia Novo[†], R. Carballo* and John V. Ringwood[‡]

*Hydraulic Engineering, University of Santiago de Compostela

Campus Universitario s/n, 27002, Lugo, Spain

[†]Nagasaki Marine Industry Cluster Promotion Association

1-43 Dejima-machi, Nagasaki 850-0862, Japan

[‡]Centre for Ocean Energy Research, Maynooth University

Maynooth, Co. Kildare, Ireland

Abstract—Flow turbulence stands out as one of the main issues that must be addressed for tidal stream energy to become a fully-fledged renewable energy source. In this context, the present paper studies the impacts on the turbulence conditions derived from the operation of a tidal energy farm. For this purpose, a 3D hydrodynamic model was implemented for the Orkney region (N Scotland), which was validated against field data of tidal flow velocity and turbulence kinetic energy (TKE). After validation, the model was used to assess the impacts on the TKE for a complete tidal cycle. The results obtained highlight the remarkable effects of tidal stream exploitation in the turbulence conditions, especially at the deepest layers of the water column, with differences up to 50 % with respect to the undisturbed conditions. Therefore, these important modifications in the turbulence conditions may increase the fatigue and loads on the mooring and supporting structures of the tidal turbines and also impact other relevant coastal processes such as pollutant and nutrient transport.

Index Terms—TEC, Orkney Region, Turbulent Kinetic Energy, Delft3D

I. INTRODUCTION

Over the last decades the aim of increasing the importance of renewable energy sources in the energy mix [1], has brought a great deal of attention into the marine energies due to its large energy potential [2]. Among them is tidal stream energy, which taps the kinetic energy of the currents caused by the tide. Tidal stream power presents significant advantages in comparison with other sources of renewable energy: (i) the resource can be predicted in advance thanks to the astronomical nature of the driving force; (ii) the load factor is comparatively high due to the properties of the fluid; and (iii) land occupation is minimal [3], [4].

This growing interest in tidal stream energy has translated into a large number of tidal resource assessment studies all over the world [3] and the development of a great variety of Tidal Energy Converters (TECs) [4]. However, and despite all the efforts both in the research and commercial communities, tidal stream energy is still in its infancy, with multitude of issues that must be addressed in detail for tidal stream energy to become a fully-fledge energy source.

One of the key aspects, which must be fully understood is the response of TECs under harsh marine environments. The most suitable sites for the exploitation of the tidal stream

energy resource are mainly located near the coast and in relatively shallow areas, where phenomena such as hydrodynamic instability due to surface waves, instability of horizontal mesoscale flows due to tidal oscillations, instability of velocity gradients in internal waves, instability of velocity gradients in the bottom boundary layer or interaction with the coast are crucial. For this reason, besides biofouling or corrosion, turbulence has been one of the most important difficulties encountered in TEC testing.

On these grounds, many authors have studied the influence of the turbulence on TEC performance. Additionally to the hydrodynamic loads on the turbine blades [5], differences in the generated wake, power and thrust coefficient have been found. According to [6], for tidal flows with low turbulence intensities, the velocity deficit generated in the flow downstream the turbines was noticeable even at a distance of 10 rotor diameters, while for flows with high values of turbulence intensity, the wakes generated by the tidal turbines were irrelevant at distances of approximately 5 rotor diameters. In addition, Blackmore [7], from laboratory tests with a 0.8 m diameter turbine observed variations of over a 10% in the peak power coefficient. Finally, in recent years, the effects of the turbulence conditions could be also noticed for full scale converters under real sea conditions [8].

In this context, the present study aims to provide meaningful insight into the alterations of the turbulence conditions derived from the operation of different configurations of tidal arrays, by means of numerical modelling. For this purpose, the Orkney region was used a case study. Due to its large energetic potential [9], the European Marine Energy Centre (EMEC) has set up several test sites, providing the opportunity to test full-scale grid-connected prototype devices for both wave and tidal conditions [10]. Regarding tidal stream energy, two test sites are available: (i) the Fall of Warness (Figure 1) a grid-connected facility, which offers five test berths at depths ranging from 25 m to 50 m in an area of approximately 8 km² and (ii) the scale tidal test site at Shapinsay Sound (Figure 1), a non-grid connected tests site, which provides TEC developers with the opportunity to test their prototypes in real sea conditions. In addition, the complex bathymetry of the region with multiple islands and channels result in

strong turbulent flows. For all the above mentioned reasons, this region appears as an excellent location to evaluate the far-field impacts of tidal stream energy exploitation on the turbulent conditions of a tidal flow.

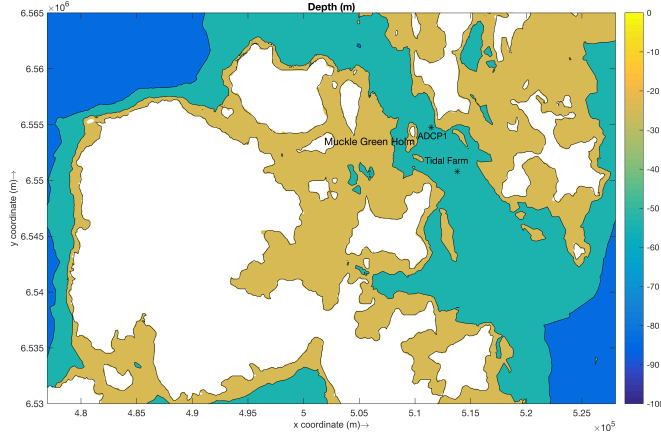


Fig. 1: Area of study: Orkney Region.

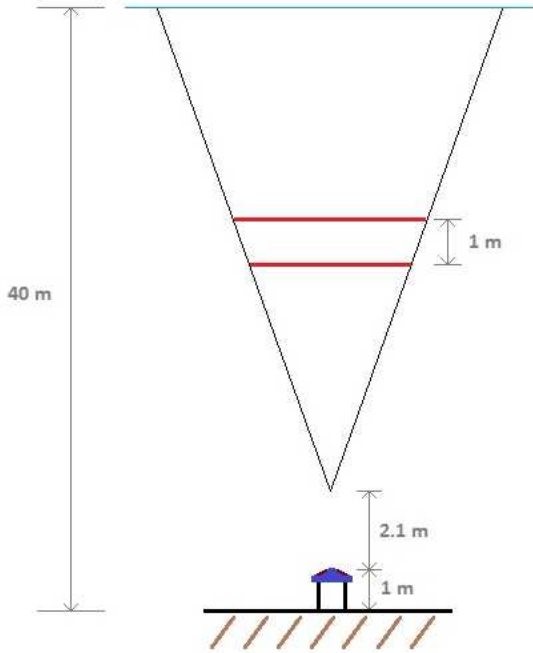


Fig. 2: Schematic representation of the ADCP installation.

II. MATERIALS AND METHODS

A. Field data. ADCP measurements

Tidal stream velocity data was collected by means of an ADCP deployed at the Fall of Warness (EMEC tidal test site, 59° 07' N, 02° 48' W) from April 3rd to May 11th, 2009. The local water depth at the deployment location is 40 m, according to the chart datum. The head of the ADCP, an RDI Workhorse Sentinel 600 kHz, was situated 1 m above the seabed. The blanking distance was set as 2.1 m and the layer width 1 m. Thus, velocity data for east, north and

vertical components were obtained for 35 vertical layers, with a sampling frequency of 0.2 Hz. Fig. 2, presents a schematic representation of the ADCP installation.

The data obtained from the ADCP was used to determine the turbulence flow conditions in the area of study. The Turbulent Kinetic Energy (TKE) density related parameter, S , was computed as follows:

$$S = \frac{1}{1 + \alpha} \left(1 + \frac{2\alpha}{\tan^2 \theta} \right) \left(\frac{q^2}{2} \right), \quad (1)$$

where, θ is the beam inclination from the vertical (20° for the present study) and $\frac{q^2}{2}$ stands for the TKE density, which can be calculate as:

$$\frac{q^2}{2} = \frac{\overline{u'^2} + \overline{v'^2} + \overline{w'^2}}{2}, \quad (2)$$

where, $\overline{u'}$, $\overline{v'}$ and $\overline{w'}$, represent the variances of the flow velocity in the x , y and z directions, respectively.

Finally, α is a turbulence anisotropy ratio, defined by Lu and Lueck [11] (Ec. 3). For the present work, α values were calculated from the measured data for every 10-minute period.

$$\alpha = \frac{\overline{w'^2}}{\overline{u'^2} + \overline{v'^2}}, \quad (3)$$

B. Delft3D-Flow numerical model

Delft3D-Flow is a finite difference code [12], which solves the unsteady shallow water equations in two (depth-averaged) or in three dimensions. The system of equations consists of the horizontal and vertical equations of motion, the continuity equation, and the transport equation for conservative constituents. The flow is forced by the tide at the open boundaries, wind stress at the free surface, pressure gradients due to free surface gradients (barotropic) or density gradients (baroclinic). Source and sink terms are included in the equations to model the discharge and withdrawal of water. Thus, the main equations solved by the model are:

(i) The continuity equation:

$$\frac{\partial u}{\partial x} + \frac{\partial v}{\partial y} + \frac{\partial w}{\partial z} = Q, \quad (4)$$

where, x , y and z represent the east, north and vertical axes, respectively; u , v and w are the velocity components on the x , y and z directions, respectively; and Q represents the intensity of mass sources per unit area.

(ii) The momentum equations in the horizontal direction:

$$\frac{Du}{Dt} = fv - g \frac{\partial \zeta}{\partial x} - \frac{g}{\rho_0} \int_{z'=z}^{z'=\zeta} \frac{\partial \rho}{\partial x} dz' + \nu_h \left(\frac{\partial^2 u}{\partial x^2} + \frac{\partial^2 u}{\partial y^2} \right) + \nu_v \left(\frac{\partial^2 u}{\partial z^2} \right), \quad (5)$$

$$\frac{Dv}{Dt} = -fu - g \frac{\partial \zeta}{\partial y} - \frac{g}{\rho_0} \int_{z'=z}^{z'=\zeta} \frac{\partial \rho}{\partial y} dz' + \nu_h \left(\frac{\partial^2 v}{\partial x^2} + \frac{\partial^2 v}{\partial y^2} \right) + \nu_v \left(\frac{\partial^2 v}{\partial z^2} \right), \quad (6)$$

where, ζ stands for the free surface elevation relative to a reference plane ($z = 0$), g is the gravitational acceleration, ρ and ρ_0 are the density and reference density of sea water, respectively; f is the Coriolis parameter and ν_h and ν_v are the horizontal and vertical eddy viscosity coefficients, respectively.

(iii) The momentum equation in the vertical direction:

Under the shallow-water assumption, the conservation of momentum in the vertical direction is simplified to the hydrostatic pressure, p , distribution:

$$\frac{\partial p}{\partial z} = -\rho g, \quad (7)$$

(iv) The transport equation:

$$\frac{Dc}{Dt} = D_h \left(\frac{\partial^2 c}{\partial x^2} + \frac{\partial^2 c}{\partial y^2} \right) + D_v \frac{\partial^2 c}{\partial z^2} - \lambda_d c + R_s, \quad (8)$$

where, c represents either salinity or temperature, λ_d represents a first order decay process, D_h and D_v are the horizontal and vertical eddy diffusivity coefficients, respectively; and, finally, R_s is the source term per unit area.

At the sea-bed, the shear stress is computed by using a quadratic stress law:

$$\vec{\tau}_b = \frac{\rho_0 g |\vec{u}_b| \vec{u}_b}{C_{3D}^2}, \quad (9)$$

where \vec{u}_b is the horizontal velocity in the bottom layer and C_{3D} is the 3D-Chezy coefficient, which is calculated from the two-dimensional Chezy coefficient, C_{2D} , as follows:

$$C_{3D} = C_{2D} + \frac{\sqrt{g}}{\varkappa} \ln \frac{\Delta z_b}{2H}, \quad (10)$$

where Δz_b represents the vertical distance from the seabed to the nearest computational grid point, \varkappa is the von Karman constant ($\varkappa = 0.41$) and H is the total water depth. Finally, C_{2D} , is computed by means of the Manning coefficient, n :

$$C_{2D} = \frac{\sqrt[6]{H}}{n} \quad (11)$$

and the wind stress exerted on the free surface is computed as follows:

$$\vec{\tau}_s = C_d \rho_a |\vec{U}_{10}| \vec{U}_{10}, \quad (12)$$

where \vec{U}_{10} represents the wind velocity vector at 10 m height above the sea surface, ρ_a is the air density, and C_d is a dimensionless drag coefficient. According to Smith [13] for wind velocities below 6 ms^{-1} .

$$C_d = 1.1 \cdot 10^{-3}, \quad (13)$$

while, according to Yelland [14] for wind velocities over 6 ms^{-1} :

$$C_d = (0.50 + 0.0071U_{10}) \cdot 10^{-3}, \quad (14)$$

Finally, in order to account for the vertical turbulent viscosity and diffusivity four options are provided: κ - ϵ , κ -L, algebraic and constant model. In this case the κ - ϵ was used with the default formulation and parameters.

C. TEC modelling in Delft3D-Flow

Delft3D-Flow presents the so-called "Porous Plate" tool [12], which can be used to simulate the operation of a TEC [15] by adding two momentum sink terms (M_x , M_y) into the right-hand side of the momentum equations (Eq. 5 and 6), which account for the loss of momentum of the flow due to the presence of the TECs. The added momentum terms can be expressed as [12]:

$$M_x = -c_{loss-x} \frac{u^2}{\Delta x}, \quad (15)$$

$$M_y = -c_{loss-y} \frac{v^2}{\Delta y}, \quad (16)$$

where the coefficients c_{loss-x} and c_{loss-y} must be defined during the setup process of the model. In this case, the methodology defined in [16], [17], which relates the c_{loss} coefficients with the thrust coefficient (C_t) exerted by a TEC was used. Consequently, c_{loss} coefficients can be defined as:

$$c_{loss-x} = \frac{-2\gamma_x}{(1 + \sqrt{1 - \gamma_x})^2}, \quad (17)$$

$$c_{loss-y} = \frac{-2\gamma_y}{(1 + \sqrt{1 - \gamma_y})^2}, \quad (18)$$

with

$$\gamma_x = \frac{C_t A_t \sin \theta}{n \Delta y \Delta z}, \quad (19)$$

$$\gamma_y = \frac{C_t A_t \cos \theta}{n \Delta x \Delta z}, \quad (20)$$

where A_t is the total area occupied by the TEC, θ is the angle between the x direction and the TEC axis (Figure 3), n is the number of vertical layers of the model occupied by the TEC, C_t is the thrust coefficient of the TEC, Δx and Δy are the grid sizes in the x and y directions, respectively. Finally, it is important to point out that this approach presents some limitations related to the discretisation of the TEC, which are highlighted in [16].

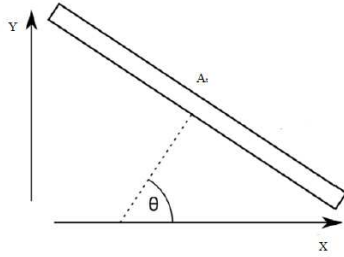


Fig. 3: Schematic representation of a TEC for Delft3D implementation

D. Model implementation

With regards to the forcing factors of the model, only astronomical and Coriolis forcing were included in the model set-up. For the boundary conditions of the model, a nesting approach was used. The coarse model was implemented in a Cartesian grid with a resolution of $250 \times 250 \text{ m}$. At the ocean boundaries the sea level was prescribed as a function of time using the major tidal harmonics (M2, S2, N2, K2, K1, O1, P1, Q1, MF, MM, M4, MS4, MN4), which were obtained from the database TPXO 7.2, a global model of ocean tides that solves the Laplace equations using data from tide gauges and the TOPEX/Poseidon Satellite [18]. On the other hand, the nested model was implemented in 3D using the σ -layer approach for the vertical discretisation. In this case, a uniform distribution of five σ -layers was prescribed, using a homogeneous thickness for all the layers corresponding with 20 % of the local water depth. Regarding the horizontal discretisation, a Cartesian grid was also used, covering the area corresponding with the proposed tidal farm in Figure 1, with a constant grid size of $25 \times 25 \text{ m}$, which allows for an accurate representation of the shorelines and bathymetry. The boundary conditions consisted of time-series of the free surface elevation, which were obtained from the coarse model. Finally, the bathymetric data for the region was obtained from the British Oceanographic Data Center (BODC) through the bathymetric data sets contained in the General Bathymetric Chart of the Oceans (GEBCO), which were interpolated onto the computational domains of the models by means of the Delft3D-QUICKIN toolbox.

III. RESULTS

A. ADCP data analysis

First of all, the collected data was subjected to a quality control based on a correlation count analysis. Then, a rotation of 4.35° to the East was made to correct the difference between magnetic and geographic north. The data resulting of this preliminary analysis was divided in 10-minute data sets, each containing 120 values. On this basis, hodographs for East and North velocity components were generated for a first velocity magnitude and direction analysis with Figure 5 showing the results obtained at 30 m , 20 m , 10 m and 4 m from the sea bottom, respectively.

With respect to the flow direction, it can be observed a clear NW-SE trend during the ebb and flood tidal cycles.

Although this behaviour is conserved throughout the water column, it can also be observed that in the deepest layers the flow direction shifts to a more N-S direction. In addition, deviations with respect to the vertical axis range from 1 deg to 10 deg for the flood tidal cycles, while in the ebb cycles varies from 13 deg to 17 deg.

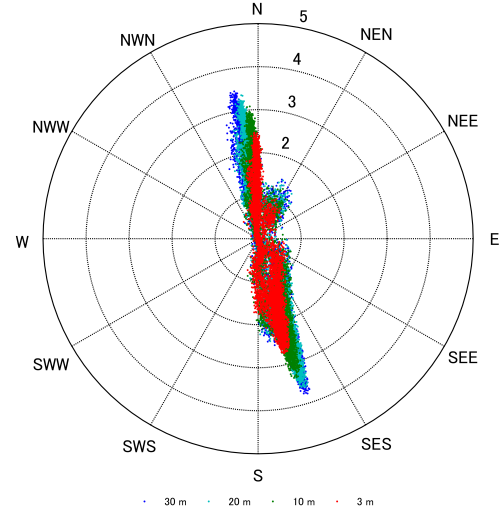


Fig. 5: Hodograph of the area of study.

Finally and based on the results shown by the hodograph two facts can be highlighted. Firstly, for the flood tides, there is a group of points that lies on the range of 0 to 1.5 ms^{-1} with a flow direction of 30 deg (clockwise from the North). However, this behaviour fades with the water depth, which may be explained by a surface eddy generated by the Muckle Green Holm Island for low velocity conditions. Secondly, a high dispersion can be observed during ebb tides for velocities below 2.5 ms^{-1} (1.75 ms^{-1} for the deepest layer), with a difference of almost 30 deg between the two extremes. Therefore, these two combined facts give a first idea of the important turbulence conditions present in the area of study.

B. Model validation

In order to ensure that the models accurately predict the hydrodynamic conditions of the area of study, they were validated by comparing the numerical results and measured data of the flow velocity and the turbulence kinetic energy (TKE). The validation was carried out at the different levels of the water column, which correspond with the upper, middle and bottom layers of the numerical model, with the validation period covering from the 07 April 2009 to 09 April 2009. Prior to the validation period, the model was spun up during a time interval of two weeks with the purpose of adjusting the flow field (generating a hot-start input file for the model), so that the initial conditions do not affect the numerical results during the period of interest.

The validation results for the flow velocity and TKE are shown in Figures 4a and 4b, respectively. Figure 4a shows

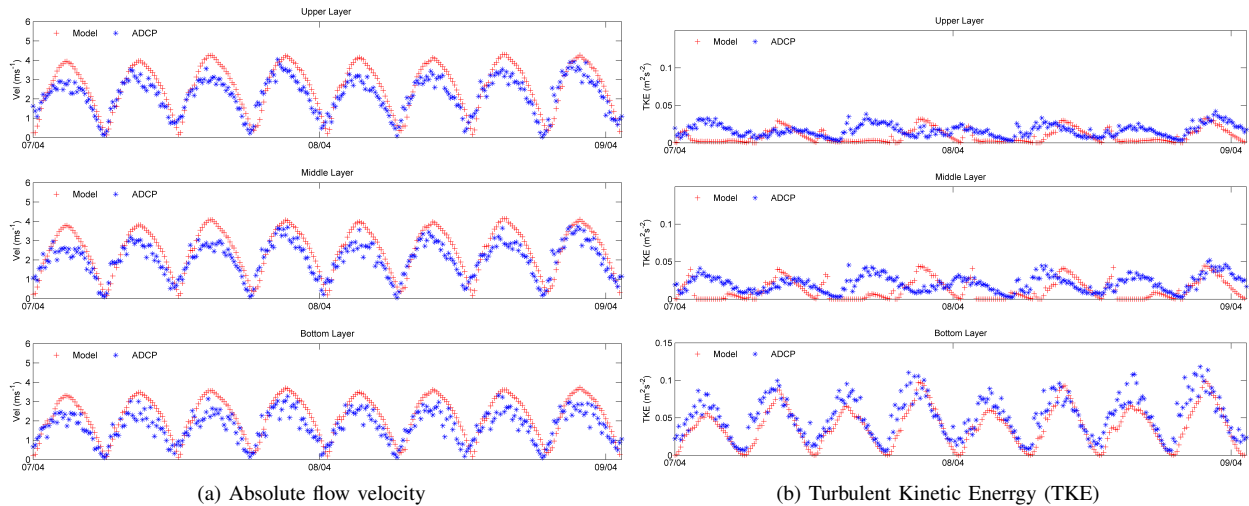


Fig. 4: Model validation results

a comparison between the time-series of the measured and computed values of the absolute flow velocity for all the different layers considered. Overall, an excellent agreement was found, with only minor differences in the peak velocities, where the model seems to slightly overestimate the peak tidal flows. With regards to the TKE the procedure presented by Togneri [19] was used for the present work, where the turbulence model was validated by comparing the TKE results from the simulation with the measured TKE density related parameter, S (Section II-A). Figure 4b shows the time-series of the computed and measured values of TKE. A remarkable agreement was found for the bottom layer, while for the middle and upper layers the measured and computed peak values of the TKE are quite similar; however, some disagreements in the phase of the two signals can be noticed. The statistical parameters of the validation are summarised in Table I, which in general terms, confirm the ability of the model to predict the flow conditions of the region.

C. Effects of a tidal stream energy exploitation on turbulence conditions

Upon validation, the model was used to assess the impacts on the turbulence conditions (TKE) in the area of study derived from tidal stream energy exploitation. For this purpose, two scenarios were considered: (i) the operation of a single TEC (T1 in Figure 6) and (ii) the operation of a tidal farm (Figure 6), using the Evopod Turbine [20], whose main characteristics are summarised in Table II, as reference. For this purpose, the flow conditions of the Fall of Warness tidal test site were used as case study (Figure 1). For the tidal farm, a triangular distribution was chosen, with the rows separated 100 m (five-diameter) from each other (in the NW-SE direction) and a lateral separation of 60 m (three-diameter) among the turbines of the same row (in the SW-NE direction) (Figure 9). This area presents an outstanding tidal resource as can be observed in Figure 6, with homogeneous flow velocities exceeding 3.5

ms^{-1} and $2.2 ms^{-1}$ at mid-ebb and mid-flood of a mean-spring tide, respectively [21].

	RMSE TKE ($m^2 s^{-2}$)	RMSE Vel (ms^{-1})
Upper layer	0.0202	0.7285
Middle layer	0.0185	0.7340
Bottom layer	0.0138	0.7476

TABLE I: Main validation statistical parameters

Evopod Turbine	
Diameter (m)	20
Cut-in velocity (ms^{-1})	0.7
Cut-off velocity (ms^{-1})	4.4
Rated velocity days (ms^{-1})	3.15
Rated power (kW)	1680

TABLE II: Main characteristics of the Evopod Turbine

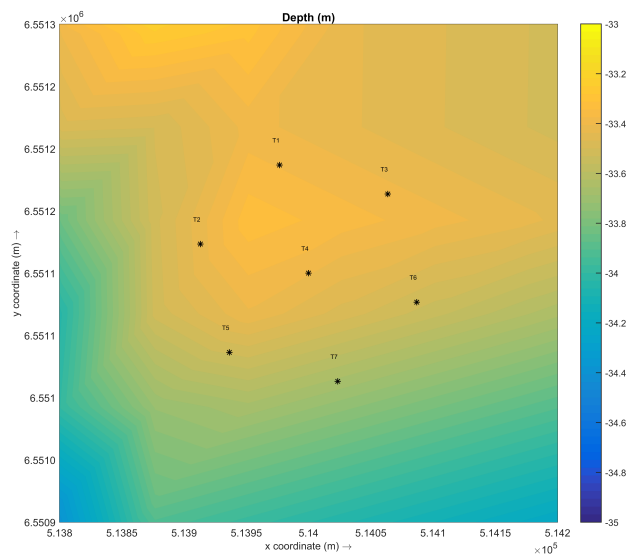


Fig. 9: Tidal farm layout

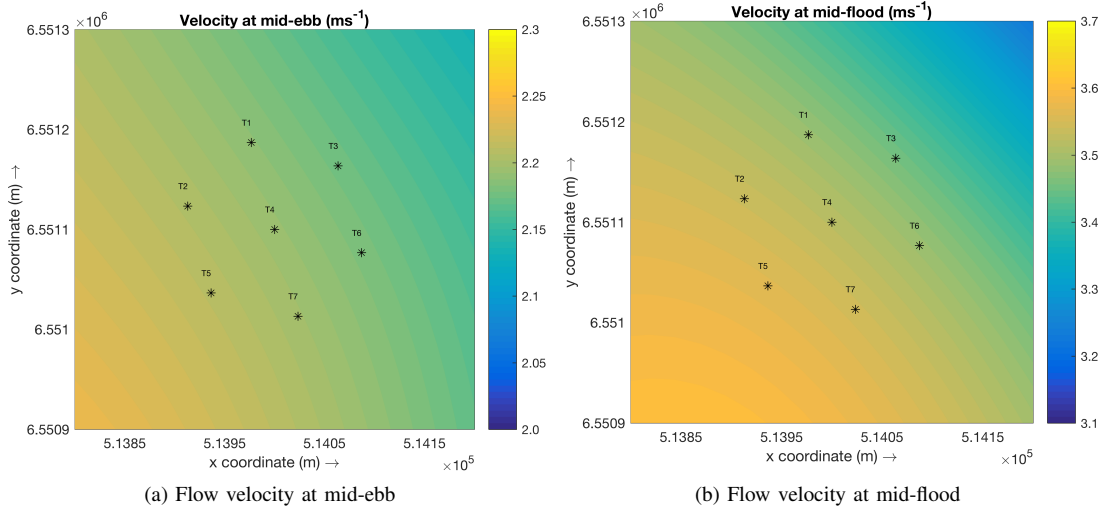


Fig. 6: Flow velocities at the tidal stream farm

Once the location and configuration of the tidal farm were defined, the model was run with and without considering the operation of the tidal turbines (energy extraction and baseline cases, respectively), for a period corresponding with a complete tidal cycle (i.e. approximately 12h). As indicated in Section III-B, a spin up period of two weeks was considered for the simulations. The operation of the Evopod turbines in Delft3D was modelled according to the methodology presented in Section II-C, considering that the tidal turbines span

3 vertical σ -layers (σ -layers 2, 3 and 4) and assuming a constant value of the thrust coefficient C_t of 0.85 [21]. The effects on the TKE (in terms of magnitude) were investigated by plotting the time-series of TKE at each individual turbine for the energy extraction and baseline cases.

Figure 7 shows the TKE differences for the case of the single Evopod Turbine for two points located one diameter upstream and downstream the turbine. Overall, it can be observed that the operation of the tidal turbine results in an increase of the TKE, which is especially noticeable in the bottom

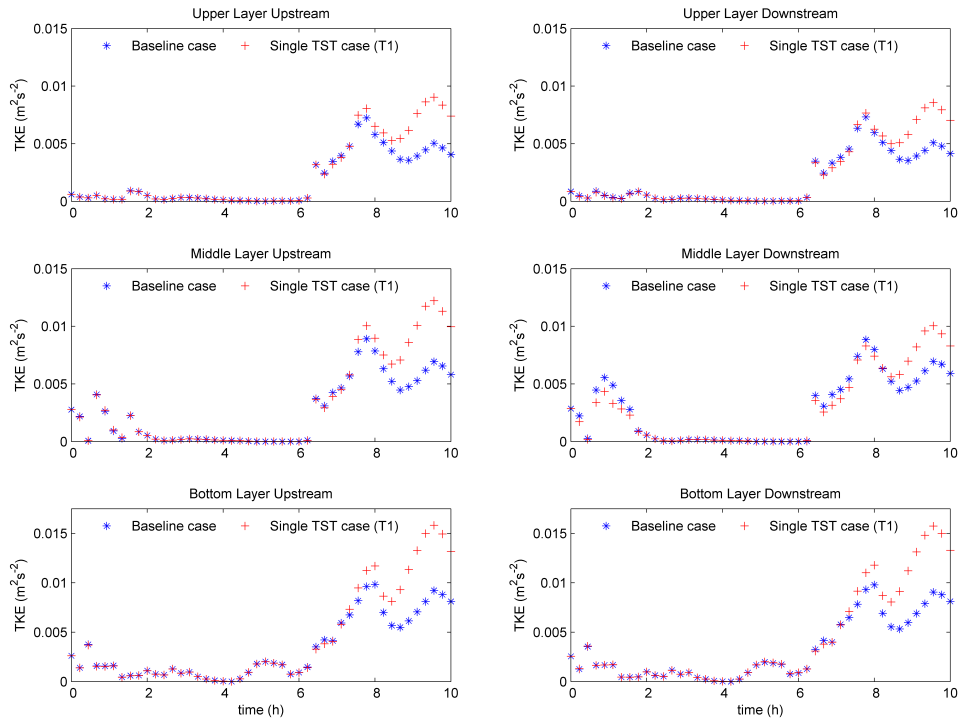


Fig. 7: Time-series of TKE for the single turbine case

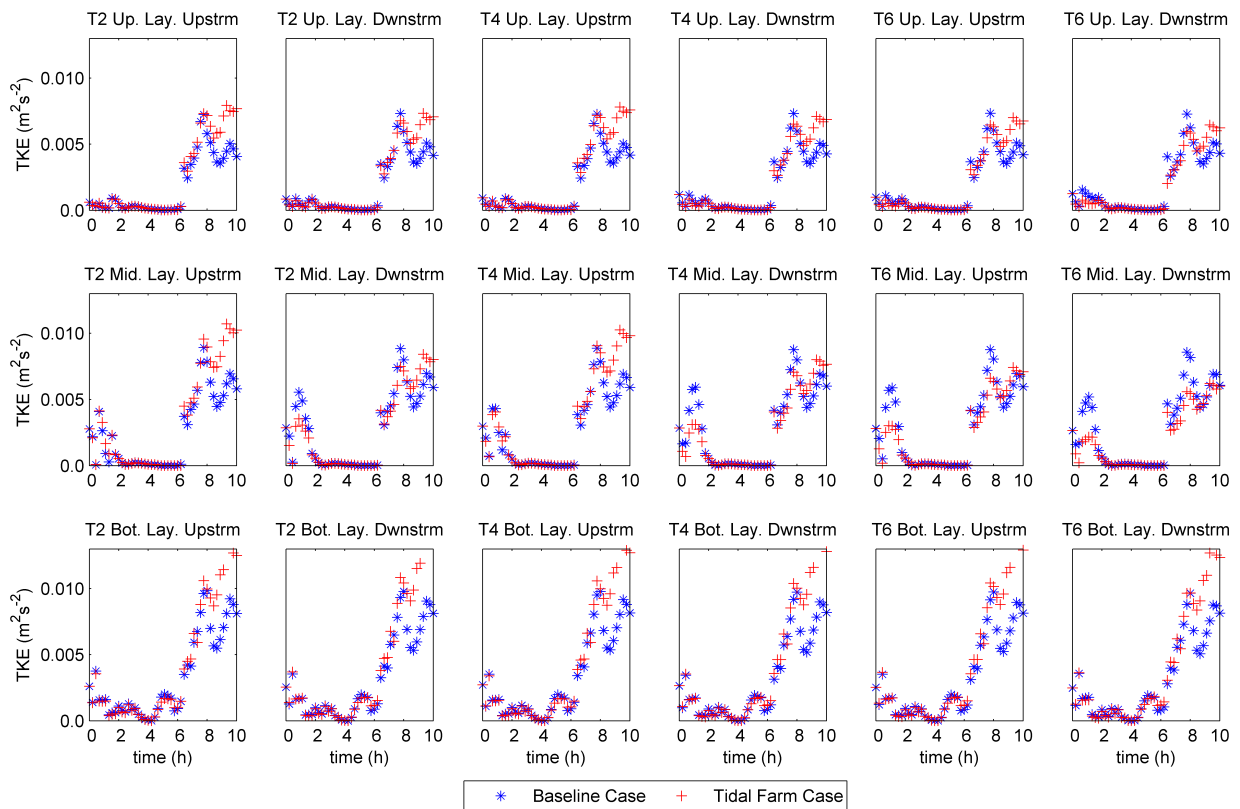


Fig. 8: Time-series of TKE for the Tidal Farm case

layer, with differences close to 50%. In the upper layers, the differences are not quite significant reaching values up to 35% and 25%, for the middle and upper layers, respectively. Due to the blockage effect exerted by the tidal turbine, the flow is forced to pass through the bottom layer, which in conjunction with the sea bed presence may explain the noticeable increase of the TKE observed in the bottom for the energy extraction case. Finally, no significant differences are found between the points located upstream and downstream the turbine.

For the tidal farm scenario, the behaviour of the TKE was studied both upstream and downstream of turbines T2, T4 and T6 (Figure 6), which are located at the three different rows of the tidal farm. The results obtained are summarised in Figure 8. Overall, a similar behaviour than the single turbine case was observed, with the TKE increasing significantly with the water depth, especially for the energy extraction case. However, it is important to point out that for turbines T4 and T6, which are located in the second and third row, respectively; the variations on the TKE are more significant, which may be explained by the modifications on the flow patterns due to the park effects of the tidal farm.

IV. CONCLUSIONS

In recent years, the interest in harvesting the tidal stream energy resource has risen sharply. However, tidal stream energy exploitation poses an enormous technological challenge, as result of the harsh environments in which Tidal Energy

Converters (TECs) are deployed. Therefore, the aim of this work is to explore the effects of the tidal stream energy exploitation on the local turbulence conditions derived from the modifications caused in the flow by the presence of a TEC or a tidal farm. On these grounds, the Orkney Region, which appears as the most promising location in Europe to exploit the tidal stream energy resource, was used as case study.

The results obtained in the present study show significant impacts on the turbulence conditions derived from the operation of a tidal farm, especially at the deepest layers of the water column. This fact is not irrelevant, since an increase in the TKE (up to 50% for the present case study) may derive into an increase of the loads and fatigues on the mooring and supporting structures of the tidal turbines. In addition, the far-field effects on the turbulence patterns may affect other relevant marine and coastal processes such as nutrient and pollution dispersion.

In summary, this work explores the main effects on the turbulence conditions due to the operation tidal stream turbines. However the results obtained should be taken as a first approximation due to the limitations when modelling the operation of a tidal turbine within a far-field hydrodynamic model (i.e. Delft3D-Flow). Additionally, alternative aspects such as the influence of different tidal farm layouts or the far-field impacts on the turbulence patterns were not considered, since, are outside the scope of this work and will be dealt with as a continuation of this research.

ACKNOWLEDGMENT

During this work, V. Ramos was supported by the I2C postdoctoral grant ED481B 2014/059-0 (Plan Galego de Investigación Innovación e Crecemento 2011-2015) of the Xunta de Galicia (Spain). The authors are also indebted to the European Marine Energy Centre (EMEC) for its contribution with the ADCP data and the Irish Centre for High-End Computing (ICHEC) for its cooperation in the computational tasks.

REFERENCES

- [1] F. O. Rourke, F. Boyle, and A. Reynolds, "Renewable energy resources and technologies applicable to Ireland," *Renewable and Sustainable Energy Reviews*, vol. 13, no. 8, pp. 1975 – 1984, 2009.
- [2] A. S. Bahaj, "Generating electricity from the oceans," *Renewable and Sustainable Energy Reviews*, vol. 15, no. 7, pp. 3399 – 3416, 2011.
- [3] R. Carballo, G. Iglesias, and A. Castro, "Numerical model evaluation of tidal stream energy resources in the Ria de Muros (NW Spain)," *Renewable Energy*, vol. 34, no. 6, pp. 1517 – 1524, 2009.
- [4] Fergal O Rourke, Fergal Boyle, and Anthony Reynolds, "Tidal energy update 2009," *Applied Energy*, vol. 87, no. 2, pp. 398 – 409, 2010.
- [5] I. Milne, A. Day, R. Sharma, and R. Flay, "The characterisation of the hydrodynamic loads on tidal turbines due to turbulence," *Renewable and Sustainable Energy Reviews*, vol. 56, pp. 851–864, 2016.
- [6] F. Maganga, G. Germain, J. King, G. Pinon, and E. Rivoalen, "Experimental characterisation of flow effects on marine current turbine behaviour and on its wake properties," *IET Renewable Power Generation*, vol. 4, no. 6, pp. 498–509, 2010.
- [7] T. Blackmore, L. E. Myers, and A. S. Bahaj, "Effects of turbulence on tidal turbines: Implications to performance, blade loads, and condition monitoring," *International Journal of Marine Energy*, vol. 14, pp. 1–26, 2016.
- [8] M. Shell, "Ieeetran homepage on ctan," 2002.
- [9] Simon P. Neill, M. Reza Hashemi, and Matt J. Lewis, "The role of tidal asymmetry in characterizing the tidal energy resource of Orkney," *Renewable Energy*, vol. 68, pp. 337 – 350, 2014.
- [10] "<http://www.emec.org.uk/>," 12 2004.
- [11] Y. Lu and R. G. Lueck, "Using a broadband adcp in a tidal channel. part ii: Turbulence," *Journal of Atmospheric and Oceanic Technology*, vol. 16, no. 11, pp. 1568–1579, 1999.
- [12] *Delft3D-FLOW user manual.*, Hydraulics, Delft., Delft, the Netherlands., 2006.
- [13] S. D. Smith, "Wind stress and heat flux over the ocean in gale force winds," *Journal of Physical Oceanography*, vol. 10, no. 5, pp. 709–726, 1980.
- [14] M. Yelland, B. Moat, P. Taylor, R. Pascal, J. Hutchings, and V. Cornell, "Wind stress measurements from the open ocean corrected for airflow distortion by the ship," *Journal of Physical Oceanography*, vol. 28, no. 7, pp. 1511–1526, 1998.
- [15] M. Sanchez, R. Carballo, V. Ramos, and G. Iglesias, "Floating vs. bottom-fixed turbines for tidal stream energy: A comparative impact assessment," *Energy*, vol. 72, pp. 691 – 701, 2014.
- [16] S. Baston, S. Waldman, and J. Side, "Modelling energy extraction in tidal flows," *MASTS Position Paper.*, vol. 1, 2015.
- [17] N. R. C. A. V. V. S. J. Waldman S, Baston S, "Implementation of tidal turbines in MIKE 3 and Delft3D models of Pentland Firth & Orkney Waters," 2016.
- [18] B. D. Dushaw, G. D. Egbert, P. F. Worcester, B. D. Cornuelle, B. M. Howe, and K. Metzger, "A topex/poseidon global tidal model (tpxo.2) and barotropic tidal currents determined from long-range acoustic transmissions," *Progress in Oceanography*, vol. 40, pp. 337 – 367, 1997, tidal Science In Honour of David E. Cartwright.
- [19] M. Togneri, M. Lewis, S. Neill, and I. Masters, "Comparison of adcp observations and 3d model simulations of turbulence at a tidal energy site," *Renewable Energy*, 2017.
- [20] OceanFlowEnergy, "<http://www.oceanflowenergy.com/>," 12 2010.
- [21] V. Ramos and J. V. Ringwood, "Implementation and evaluation of the International Electrotechnical Commission specification for tidal stream energy resource assessment: A case study," *Energy Conversion and Management*, vol. 127, pp. 66–79, 2016.